Journal of Materials Chemistry

www.rsc.org/materials

Volume 20 | Number 27 | 21 July 2010 | Pages 5553–5764

ISSN 0959-9428

RSC Publishing

Microstructure, electrocatalytic and sensing properties of nanoporous $Pt_{46}Ni_{54}$ alloy nanowires fabricated by mild dealloying†

Lifeng Liu,* Roland Scholz, Eckhard Pippel and Ulrich Gösele‡

Received 21st January 2010, Accepted 31st March 2010
First published as an Advance Article on the web 20th May 2010
DOI: 10.1039/c0jm00113a

Well-defined nanoporous $Pt_{46}Ni_{54}$ alloy nanowires were fabricated by mild dealloying of the electrodeposited Pt_4Ni_{96} nanowires, and showed a remarkably enhanced electrocatalytic activity towards methanol oxidation and good H_2O_2 sensing properties.

1. Introduction

With the worldwide ever-increasing demand for clean energy, electrocatalysts that can convert chemical energy into electrical energy have attracted more and more attention from both scientific and industrial communities. Also, there has been growing research interest in electrochemical sensors in recent years owing to the prosperous developments in the field of biochemical and clinical analyses. Nanostructured materials usually possess a high surface area and unusual chemical properties at their surfaces and interfaces, and therefore have been widely explored for possible applications in electrocatalysis and electrochemical sensing. For example, Pt-based nanostructures including nanoparticles,[1–4] nanowires,[5–7] hollow spheres[8] and nanosheets[9] have been found to exhibit enhanced electrocatalytic activity towards either the anode or cathode reaction of a polymer electrolyte membrane fuel cell (PEMFC). Gold nanoparticle films,[10] carbon nanotubes[11] and hybrid nanostructures[12,13] have also been demonstrated to be promising electrochemical sensors with high sensitivity and selectivity.

Among various nanostructured materials, nanoporous metals are especially attractive for use as electrocatalysts and electrochemical sensing materials because of the combination of very high surface area and electric contact to all surface sites.[14] In addition, nanoporous metals are well interconnected and do not require any supports so that the corrosion and de-adhesion problems that nanoparticle/support systems often suffer can be avoided. Nanoporous metals are usually prepared by dealloying a binary or multi-component alloy that contains at least one noble metal component. So far, nanoporous elemental metals such as Au,[15–20] Pt,[21–23] Pd[24] and Cu[25,26] have been extensively studied and their applications in electrocatalysis and sensing have also been explored.[27–29] However, for most electrocatalytic and electrochemical sensing applications, a nanoporous bimetallic or tri-metallic alloy structure would be more favorable because it is well known that alloys can not only reduce the loadings of precious metal (hence reduce the costs), but also improve catalytic or sensing performance of the porous structures. Chen's group reported the syntheses of a series of porous Pt-based alloy networks using a solution phase reduction route and studied their electrocatalytic properties.[30–33] Nevertheless, both the pore and ligament sizes of thus-obtained porous materials are fairly large (several hundred nanometers), which is not conducive to achieving maximum utilization of platinum. More recently, Snyder *et al.* prepared nanoporous Pt-Au-Ag ternary alloy by electrochemical dealloying,[14] the average pore size of which is only around 4 nm. Xu *et al.* also demonstrated a bimetallic mesoporous structure prepared by dealloying a Cu-Al alloy and a subsequent galvanic replacement reaction between the resulting nanoporous Cu and the Pt precursors, and observed a much enhanced electrocatalytic activity towards methanol oxidation.[34] However, nanoporous alloy structures remain largely unexplored up to now.

In our previous work, we reported the formation of nanoporous Pt-Co nanowires with different morphologies and compositions by a mild dealloying method.[35] Here, we demonstrate that the mild dealloying can be extended to prepare other porous Pt-based nanowires such as Pt-Ni. As an example, we fabricated nanoporous $Pt_{46}Ni_{54}$ alloy nanowires by dealloying the electrodeposited Ni-rich Pt_4Ni_{96} nanowires in a mild acid solution. We thoroughly characterized the as-prepared porous alloy nanowires by transmission electron microscopy (TEM), and investigated their electrocatalytic activity towards methanol oxidation as well as electrochemical sensing behavior towards hydrogen peroxide oxidation. Our results showed that the nanoporous $Pt_{46}Ni_{54}$ alloy nanowires not only show a remarkably enhanced catalytic activity in comparison to the state-of-the-art Pt/C and PtRu/C commercial catalysts, but also exhibit an even higher mass activity than the previously reported nanoporous Pt-Co nanowires with a similar Pt content. In addition, these porous $Pt_{46}Ni_{54}$ nanowires also turned out to be promising materials for hydrogen peroxide sensors.

2. Experimental

Preparation of AAO membranes

The AAO membranes were prepared by a two-step anodization process as described previously.[36] Briefly, a high purity aluminium foil (99.999%, Goodfellow, 1 mm in thickness) was first electro-polished in a mixed solution of $HClO_4$ and C_2H_5OH

Max Planck Institute of Microstructure Physics, Weinberg 2, D06120 Halle, Germany. E-mail: liulif@mpi-halle.de; Fax: +49 345 5511223; Tel: +49 345 5582902

† Electronic supplementary information (ESI) available: Calculation of the Pt loading on nanoporous $Pt_{46}Ni_{54}$ nanowire electrode. See DOI: 10.1039/c0jm00113a

‡ In memory of Prof. Ulrich Gösele.

(v/v 1 : 4). Subsequently, the aluminium foil was anodized in 0.3 M $H_2C_2O_4$ at 1 °C for 20 h, under a voltage of 40 V. Afterwards, the anodized Al foil was submerged into a mixture of 1.8 wt.% CrO_3 and 6 wt.% H_3PO_4 at 45 °C for 20 h to remove the oxidized layer. The second anodization was performed under the same conditions as the first one. A free-standing AAO membrane was obtained by a step-wise voltage reduction procedure in the same solution at 10 °C, followed by a short-time etching (<10 min) with 5 wt.% H_3PO_4 at room temperature. The average pore diameter of as-obtained AAO membranes is 45 nm.

Fabrication and characterization of nanoporous $Pt_{46}Ni_{54}$ nanowires

The nanoporous $Pt_{46}Ni_{54}$ nanowires were prepared by electrodeposition of Pt_4Ni_{96} alloy into an AAO membrane, followed by a mild dealloying treatment. Before electrodeposition, a thin Au layer was sputtered on the pore-mouth side of the through-hole AAO membrane. The electrodeposition was carried out in a standard three-electrode electrochemical cell, and was controlled by a potentiostat/galvanostat (Princeton Applied Research, 263A). The Au-coated AAO membrane and a platinum mesh were used as working and counter electrodes, respectively, and a Ag/AgCl electrode (double junction, saturate KCl) was employed as a reference. The electrolyte consisted of 0.5 M $NiSO_4$, 0.01 M K_2PtCl_6 and 0.485 M H_3BO_3. All the chemicals used were of analytical grade. The deposition was performed at room temperature at a potential of −1.0 V (*vs.* Ag/AgCl) which is favourable for the reduction of Ni^{2+}, leading to the formation of Pt_4Ni_{96} nanowires. To obtain porous nanowires, the Pt_4Ni_{96} nanowires embedded in the AAO membrane were subjected to dealloying treatment in 10 wt.% H_3PO_4 solution at 45 °C for 15 h.

The morphology and composition of the electrodeposited Pt_4Ni_{94} nanowires as well as nanoporous $Pt_{46}Ni_{54}$ nanowires were examined by a JEOL JEM-1010 and Philips CM20 FEG transmission electron microscope (TEM), and the detailed microstructure was investigated with a JEOL JEM-4010 high-resolution TEM.

Evaluation of the electrocatalytic performance

The electrocatalytic activity of the nanoporous $Pt_{46}Ni_{54}$ nanowires towards methanol oxidation was evaluated at room temperature in 1 M $HClO_4$ solution containing 1 M CH_3OH. To this end, a thick Au film (~200 nm) was sputtered on the surface of AAO membranes before electrodeposition, and a Au nanorod base electrode (~500 nm in length) was fabricated to support the dealloyed porous nanowire array. The dealloying treatment was conducted in the electrochemical cell used for electrodeposition. After dealloying, the nanoporous $Pt_{46}Ni_{54}$ nanowires were rinsed thoroughly with deionized water, and then the mixture of $HClO_4$ and CH_3OH was carefully injected into the cell. The detailed measurement scheme was described in our previous work.[35] For comparison, the electrocatalytic properties of commercially available Pt/C and PtRu/C catalysts as well as nanoporous $Pt_{42}Co_{58}$ nanowires prepared by the same method were also measured. The Pt/C (30% Pt on Vulcan XC-72, E-TEK) and PtRu/C (30% PtRu (1 : 1 a/o) on Vulcan XC-72, E-TEK) catalyst inks were prepared by adding 1.5 mg Pt/C and 2 mg PtRu/C respectively into 1 ml deionized water. Before use, the inks were subjected to ultrasonication for 30 min to make the catalysts uniformly dispersed in the solution. Afterwards, 10 μL catalyst ink was dropped onto a glassy carbon (GC) working electrode, leading to a Pt loading of ~4.5 μg for both Pt/C and PtRu/C. A platinum mesh and a Ag/AgCl electrode were employed as the counter and reference electrodes, respectively. The electrocatalytic measurements were carried out at room temperature with a 263A potentiostat/galvanostat (Princeton Applied Research) as a power source. Before formally recording a cyclic voltammogram (CV) plot, we performed potential cycling between 0 V and 1.0 V (*vs.* Ag/AgCl) for five times for the $Pt_{46}Ni_{54}$ and $Pt_{42}Co_{58}$ nanowire electrodes and ten times for both Pt/C and PtRu/C electrodes in order to achieve stable CV curves.

Electrochemical sensing tests

The electrochemical sensing measurements were carried out in a three-electrode electrochemical cell with a 0.1 M phosphate buffer solution (PBS, pH 7.4) as a supporting electrolyte. A GC electrode covering with the nanoporous $Pt_{46}Ni_{54}$ nanowires was used as working electrode, and a platinum wire and a Ag/AgCl electrode were employed as the counter and reference electrodes, respectively. During the measurements, the working electrode was biased at 0.6 V (*vs.* Ag/AgCl), and the electrolyte was stirred in order to accelerate the diffusion of H_2O_2 in the solution.

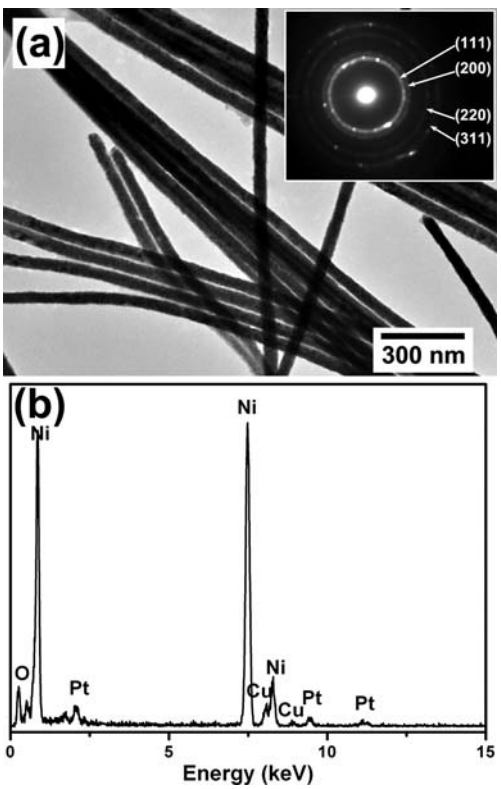

Fig. 1 (a) TEM image of as-deposited Pt_4Ni_{96} nanowires. Inset: electron diffraction pattern. (b) EDX spectrum of Pt_4Ni_{96} nanowires.

3. Results and discussion

Fig. 1a shows a representative TEM image of the electrodeposited Pt_4Ni_{96} nanowires, the starting materials for the dealloying. The nanowires are continuous and dense, and uniform in diameter along the entire wires. The average diameter of the Pt_4Ni_{96} nanowires is 45 nm, consistent with the pore size of the AAO used. The electron diffraction (ED) pattern shown in the inset of Fig. 1a exhibits only a single set of diffraction rings, which can be roughly indexed as fcc polycrystalline Ni (JCPDF 04-0850). This suggests that alloying of a small amount of Pt does not greatly change the crystal structure of Ni as a major phase. In order to determine the composition of the deposited nanowires, extensive energy-disperse X-ray spectrum (EDX) analyses were carried out, which confirmed that the as-deposited nanowires consist of Pt and Ni, and their atomic ratio is around 4 : 96 on average (Fig. 1b).

The nanoporous $Pt_{46}Ni_{54}$ alloy nanowires were successfully obtained after dealloying the Pt_4Ni_{96} nanowires in a 10 wt.% H_3PO_4 solution at 45 °C in the presence of porous alumina membranes. The detailed microstructure and composition of as-prepared porous nanowires were investigated by TEM, as shown in Fig. 2. It is evident that after dealloying, the resulting porous nanowires turned to be flexible (Fig. 2a). From Fig. 2b and c, it is seen that a large density of nanopores are distributed along the nanowires, with a pore size of 1–6 nm and a ligament width of 2–7 nm. Electron diffraction revealed that the porous nanowires are polycrystalline fcc Ni-Pt alloy (Fig. 2a, inset). The average diameter of the porous nanowires was found to be 28 nm, much smaller than that of the original Pt_4Ni_{96} nanowires (45 nm). The diameter shrinkage can be seen more clearly in Fig. 2d, in which the diameter of the short Au nanorod base electrode is in good agreement with the pore size of the AAO templates (~ 45 nm), whereas the diameter of porous nanowires is observed to reduce significantly upon dealloying. The volume shrinkage can be ascribed to the plastic deformation by homogeneous slip in small ligaments or by climb of lattice dislocations during the dealloying process.[37] Fig. 2e shows a representative EDX spectrum of the as-prepared porous nanowires, which discloses that the nanowires still consist of Pt and Ni after dealloying, and their atomic ratio is changed to 46 : 54. The Cu peaks shown in the spectrum originate from the TEM grid. It is known that dealloying is a dynamic process during which less noble metal atoms are dissolved away while noble metal atoms rapidly diffuse and re-organize at alloy/electrolyte interfaces.[15,16] The existence of a considerable amount of Ni upon dealloying can be attributed to the rapid diffusion of Pt atoms at the alloy/electrolyte interfaces, which makes the outer surface of the nanowires passivated and therefore inhibits further removal of the interior Ni.[35] A high-resolution TEM image of the as-prepared nanoporous $Pt_{46}Ni_{54}$ nanowires is shown in Fig. 2f. The visible lattice spacing is around 2.17 Å, close to that of PtNi (111) crystal planes (2.16 Å, JCPDF 65-2797). It was also noted that the crystal lattices turned out to be distorted somewhere, which may be induced by the surface stress that widely exists in dealloyed metallic nanostructures.[37,38]

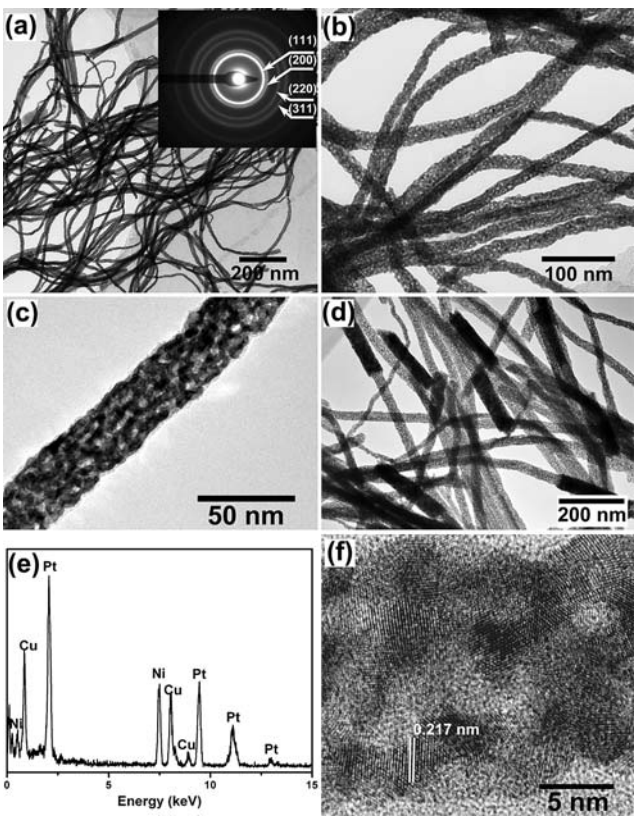

Fig. 2 TEM characterization of the nanoporous $Pt_{46}Ni_{54}$ nanowires. (a) Overview TEM picture. Inset: electron diffraction pattern. (b) Magnified TEM image. (c) A single porous nanowire. (d) Nanoporous $Pt_{46}Ni_{54}$ nanowires connected with short Au nanorods, showing the diameter shrinkage during the dealloying process. (e) EDX spectrum. (f) High-resolution TEM image.

Fig. 3 shows a typical cyclic voltammogram (CV) of the nanoporous $Pt_{46}Ni_{54}$ nanowires recorded in Ar-saturated 0.1 M $HClO_4$ solution at room temperature. For comparison, the CV curves of commercially available Pt/C and PtRu/C catalysts as well as the nanoporous $Pt_{42}Co_{58}$ nanowires are also presented. The electrochemically activated surface area (ECSA) of the

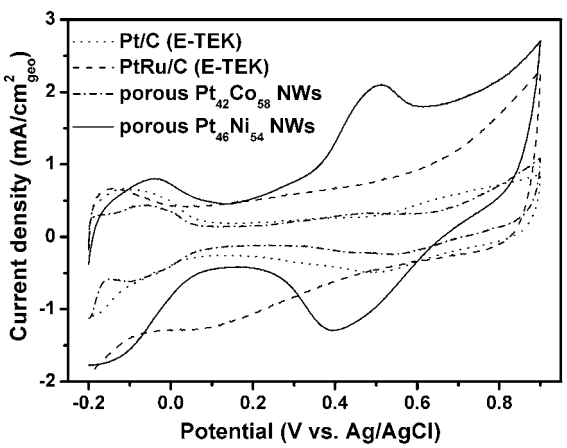

Fig. 3 Cyclic voltammograms (CVs) of the nanoporous $Pt_{46}Ni_{54}$ nanowires, Pt/C and PtRu/C commercial catalysts (E-TEK) which were recorded in Ar-saturated 0.1 M $HClO_4$ solution at room temperature. Scan rate: 50 mV/s. The CV trace of the nanoporous $Pt_{42}Co_{58}$ nanowires was reproduced from ref. 35.

catalysts can be determined from the mean charge of the hydrogen adsorption and desorption areas (from −0.2 V to 0.15 V *vs.* Ag/AgCl) by using 210 $\mu C/cm^2_{Pt}$ as the conversion factor.[39]

$$S_{ECSA} = \left(\int_{E1}^{E2} idE \right)/210\nu\rho \quad (1)$$

where ν is the potentiodynamic scan rate, $E1$ and $E2$ are the potentials at which the adsorbed hydrogen is zero and maximum, and ρ represents the Pt loading (g/cm^2). The calculated S_{ECSA} values for the nanoporous $Pt_{46}Ni_{54}$ nanowires, Pt/C and PtRu/C catalysts are 40.4 m^2/g, 36.5 m^2/g and 13.3 m^2/g, respectively, which indicates that the as-prepared porous $Pt_{46}Ni_{54}$ nanowires have a higher ECSA. Note that the ECSA of the nanoporous $Pt_{46}Ni_{54}$ nanowires is also higher than that of the nanoporous $Pt_{42}Co_{58}$ nanowires reported previously (31.1 m^2/g).[35]

The electrocatalytic performance of the nanoporous $Pt_{46}Ni_{54}$ nanowire catalysts for methanol oxidation was evaluated in a mixed solution of 1 M $HClO_4$ and 1 M CH_3OH at room temperature by cyclic voltammetry (CV) and chronoamperometry (CA). The CV and CA curves are normalized by the real Pt surface area and Pt mass, respectively, as shown in Fig. 4. The electrocatalytic performance of the porous $Pt_{46}Ni_{54}$ nanowires as well as Pt/C and PtRu/C catalysts is summarized in Table 1. It is known that PtRu is a good catalyst that can oxidize methanol at a low potential.[40] From Fig. 4, it is seen that the onset potential of the nanoporous $Pt_{46}Ni_{54}$ nanowires (~0.25 V) is close to that of PtRu/C catalysts but much lower than that of Pt/C (~0.45 V), suggesting that the oxidation of methanol is easier to accomplish with the porous nanowires catalysts. According to Fig. 4a, the specific methanol oxidation current (*i.e.* the forward sweep peak, I_f) of the nanoporous $Pt_{46}Ni_{54}$ nanowires is 5.31 mA/cm^2_{Pt}, much higher than that of Pt/C (1.36 mA/cm^2_{Pt}) and PtRu/C (3.77 mA/cm^2_{Pt}) and also higher than that of newly developed Pt/nanoporous gold (Pt/NPG, <2 mA/cm^2_{Pt})[27] and nanotubular mesoporous Pt/Cu (NM-Pt/Cu) catalysts (<2.5 mA/cm^2_{Pt}),[34] showing that the catalytic activity of the nanoporous $Pt_{46}Ni_{54}$ nanowires is intrinsically superior. The mass activity of nanoporous $Pt_{46}Ni_{54}$ nanowires was also found to be 4.3 times higher than those of both Pt/C and PtRu/C catalysts (Fig. 4b), and even higher than that of nanoporous Pt-Co nanowires with a similar Pt content ($Pt_{42}Co_{58}$, the dash dot plot in Fig. 4b), which could partly be due to the higher ECSA of the nanoporous $Pt_{46}Ni_{54}$ nanowires. Note that both the measured specific and mass activities for Pt/C are comparable to or higher than those reported before,[27,28,34,40] which means that the relative enhancements reported here are intrinsic, instead of arising from the small fiducial marks for Pt/C catalysts. The current-time plots of the nanoporous $Pt_{46}Ni_{54}$ nanowires were also recorded and compared with those of the Pt/C, PtRu/C and nanoporous $Pt_{42}Co_{58}$ nanowires, as shown in Fig. 4c and d. It is seen that the methanol oxidation current of all the catalysts decays with time because of the poisoning of the carbonaceous species. However, within the initial 1000 s, the current attenuation of the nanoporous $Pt_{46}Ni_{54}$ nanowires is only 40%; by contrast, the current of Pt/C, PtRu/C and nanoporous $Pt_{42}Co_{58}$ nanowires reduces by 85%, 73% and 84%, respectively. In addition, it is also observed that the current of the porous $Pt_{46}Ni_{54}$ nanowire electrode is higher than those of Pt/C, PtRu/C and nanoporous $Pt_{42}Co_{58}$ nanowires in the entire time range. These results indicate that the nanoporous $Pt_{46}Ni_{54}$ nanowires have a better catalytic performance for methanol oxidation.

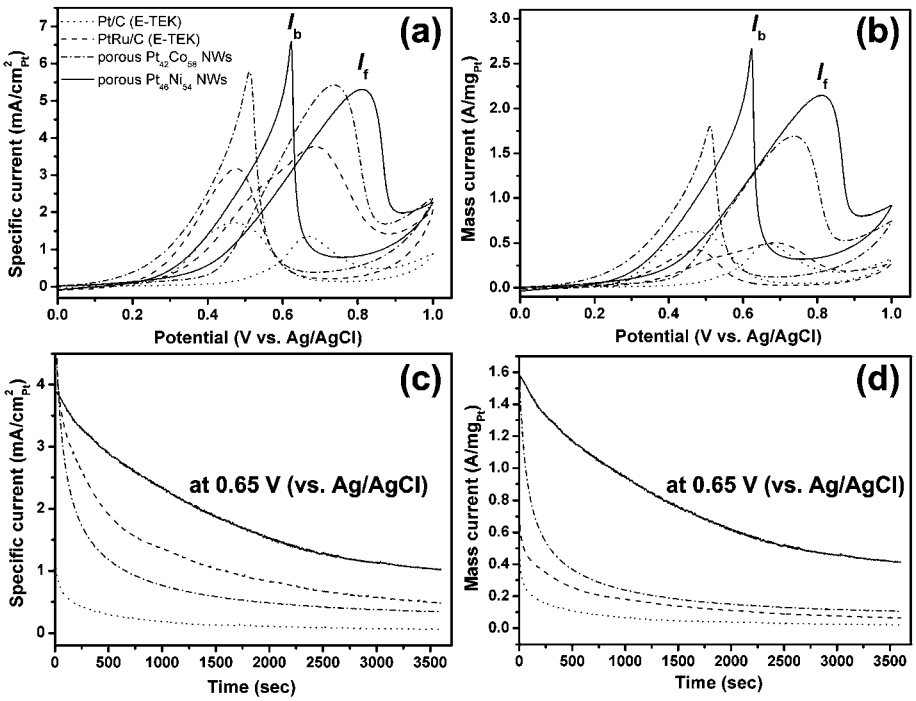

Fig. 4 Electrocatalytic performance of the nanoporous $Pt_{46}Ni_{54}$ nanowires, Pt/C and PtRu/C catalytsts. (a, b) Cyclic voltammograms, scan rate: 50 mV/s. (c, d) Chronoamperograms (CAs) recorded at 0.65 V (*vs.* Ag/AgCl). The electrolyte consisted of 1 M $HClO_4$ and 1 M CH_3OH. The CV and CA plots of the nanoporous $Pt_{42}Co_{58}$ nanowires were reproduced from ref. 35.

Table 1 Electrocatalytic performance of the Pt/C and PtRu/C commercial catalysts as well as the nanoporous $Pt_{46}Ni_{54}$ nanowires towards methanol oxidation. The real Pt surface area and electrochemically active surface area (ECSA) are calculated according to the voltammograms recorded in Ar-saturated 0.1 M $HClO_4$ solution at room temperature. The methanol oxidation currents were recorded in a mixed solution of 1 M $HClO_4$ and 1 M CH_3OH at room temperature, and normalized to the real Pt surface area and the Pt mass, respectively. The working electrode area (*i.e.* geometrical area) is 0.196 cm^2 for Pt/C and PtRu/C catalysts and 0.95 cm^2 for the nanoporous $Pt_{46}Ni_{54}$ nanowire catalysts. Scan rate: 50 mV/s. The data of the nanoporous $Pt_{42}Co_{58}$ nanowires are extracted from ref. 35

			Peak current density	
Sample	Real surface area (cm^2_{Pt}/cm^2_{geo})	ECSA (m^2/g_{Pt})	Specific (mA/cm^2_{Pt})	Mass (A/mg_{Pt})
Pt/C 30 (E-TEK)	8.38	36.5	1.36	0.49
PtRu/C 30 (E-TEK)	3.05	13.3	3.77	0.50
Nanoporous $Pt_{42}Co_{58}$ NWs	5.19	31.1	5.43	1.69
Nanoporous $Pt_{46}Ni_{54}$ NWs	12.97	40.4	5.31	2.15

It is well established that alloying of Pt with transition metals can achieve better methanol oxidation performance in comparison to pure Pt because the alloying can lower the electronic binding energy of Pt in the alloy and promote the C–H cleavage at low potential.[41] But in this work, we think that the alloying effect is not sufficient for explaining the remarkable activity enhancement of the nanoporous $Pt_{46}Ni_{54}$ nanowires as the catalytic performance of the porous $Pt_{46}Ni_{54}$ nanowires was found to be even much higher than that of the well-developed, state-of-the-art PtRu/C alloy catalysts. We therefore assume that the unique nanoporous morphology combined with the Pt-enriched outer surface should play a dominant role in the enhancement of methanol oxidation activity of the nanoporous $Pt_{46}Ni_{54}$ nanowires. On one hand, the high surface area of the porous $Pt_{46}Ni_{54}$ nanowires offers multiple adjacent active Pt sites which are necessary for the methanol dissociation and electron transfer, thus is favourable for the oxidation of methanol. On the other hand, almost all surface sites of the porous nanowires are highly conductive because of the Pt-enriched nature of the wire surfaces, which can facilitate the reaction kinetics of the electrocatalysis and therefore lead to an enhancement in activity. Additionally, the strains, which widely exist in dealloyed porous materials, may also contribute to the activity enhancement according to previous studies on porous Pt-based alloys.[1,42]

We also examined the structural stability of the nanoporous $Pt_{46}Ni_{54}$ nanowires after multiple CV and CA measurements. Fig. 5 shows typical TEM pictures of the porous nanowires subjected to 10 cycles of CV recording and subsequent 1 h CA testing. It is evident that there is no dramatic morphology change with the porous nanowires except the slightly widened nanopores and reduced ligament width. Moreover, electron diffraction investigation confirmed that the porous nanowires remained crystalline after methanol oxidation tests and can still be assigned as PtNi alloy.

In addition to remarkably enhanced electrocatalytic performance towards methanol oxidation, the as-prepared nanoporous $Pt_{46}Ni_{54}$ nanowires also exhibit good sensing performance towards the oxidation of H_2O_2, an essential mediator in food, pharmaceutical, clinical and environmental industries.[43] Fig. 6 shows typical CV traces of a porous $Pt_{46}Ni_{54}$ nanowire modified GC electrode in a 0.1 M phosphate buffer solution (PBS, pH 7.4) in the absence and presence of H_2O_2. It is seen that the porous nanowire modified electrode exhibits a higher oxidation current starting from 0.2 V (*vs.* Ag/AgCl) in the presence of 5 mM H_2O_2, and the current plateau appears at around 0.6 V (*vs.* Ag/AgCl).

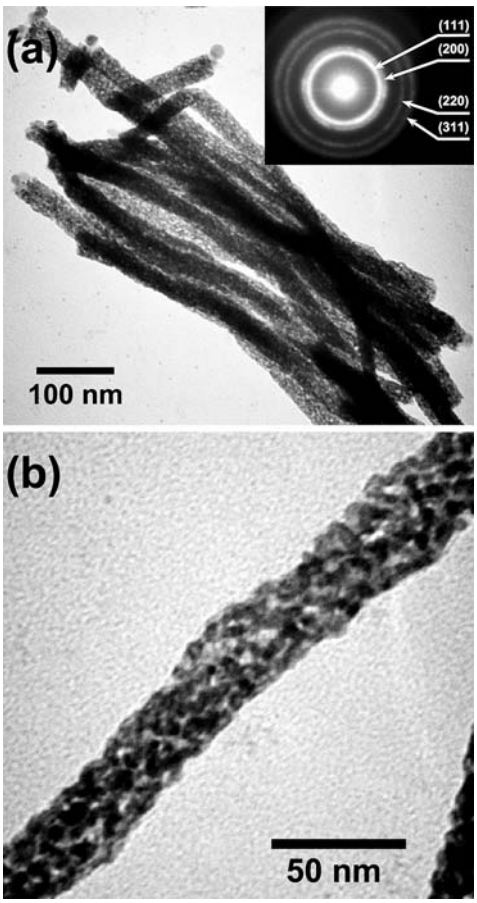

Fig. 5 TEM pictures of the nanoporous $Pt_{46}Ni_{54}$ nanowires after methanol oxidation tests (10 CV measurements between 0 and 1 V and 1 h catalytic oxidation of methanol at 0.65 V). The electrolyte consisted of 1 M $HClO_4$ and 1 M CH_3OH.

Fig. 7a displays a representative current-time response of the porous nanowire modified GC electrode to the successive addition of H_2O_2 into the stirring PBS at an applied potential of 0.6 V. It can be seen that the electrode responses quickly to each addition of H_2O_2, and the current usually reaches a steady-state within 5 s. The fast response could be ascribed to the easy diffusion of H_2O_2 into the porous nanowires and the Pt-enriched outer surface of the nanoporous $Pt_{46}Ni_{54}$ nanowires. Fig. 7b represents a plot of H_2O_2 oxidation current as a function of H_2O_2

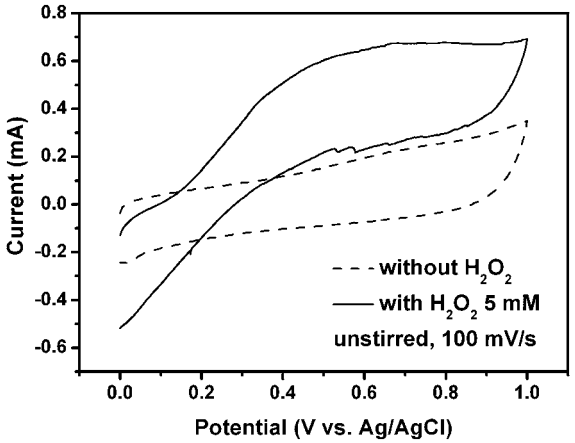

Fig. 6 Cyclic voltammograms of the nanoporous $Pt_{46}Ni_{54}$ nanowire modified glassy carbon electrode in the absence and presence of 5 mM H_2O_2. Scan rate: 100 mV/s.

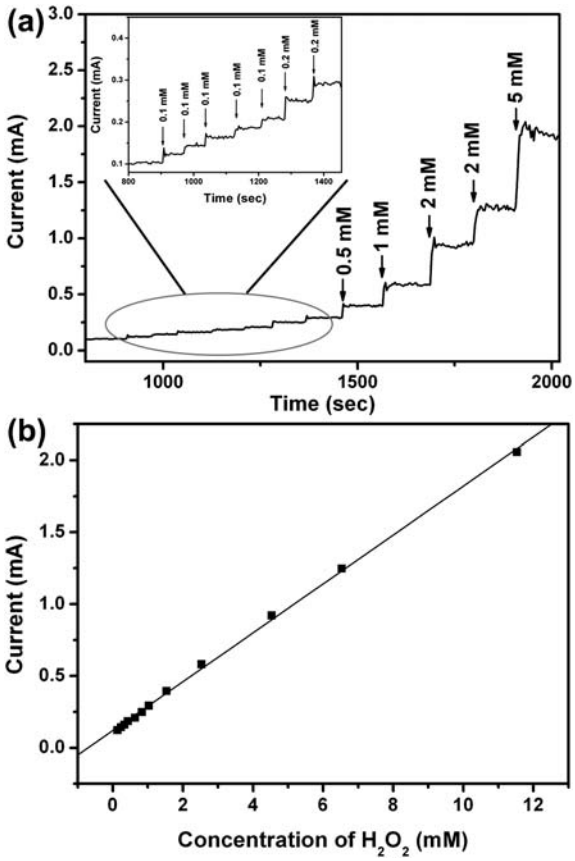

Fig. 7 (a) Current-time response of the nanoporous $Pt_{46}Ni_{54}$ nanowire modified GC electrode to the successive addition of H_2O_2 into the stirring PBS (pH 7.4). (b) The plot of catalytic oxidation current of H_2O_2 as a function of its concentration. The solid line represents the linear fit of the data.

concentration. The porous nanowire modified electrode reveals a linear current response ranging from 0.1 mM to 12 mM with a correlation coefficient of 0.9986 and a slope of 0.17 mA/mM. The detection limit of the porous $Pt_{46}Ni_{54}$ nanowire modified GC electrode is 0.1 mM, which is higher than that of a nanofiber/nanoparticle hybrid nanostructure modified GC electrode[12,13] and silver nanoparticle assemblies[44] but lower than that of silver macro-electrode[45] and carbon nanotube modified GC electrode.[46,47]

4. Conclusions

In summary, we synthesized nanoporous $Pt_{46}Ni_{54}$ nanowires by dealloying the electrodeposited Pt_4Ni_{96} nanowires in a mild acid solution. As-prepared nanowires exhibit a well-defined porous structures with a pore size of 1–6 nm and ligament width of 2–7 nm. Electrocatalytic measurements reveal that the nanoporous $Pt_{46}Ni_{54}$ nanowires exhibit remarkably enhanced activity towards methanol oxidation, showing substantial promise as efficient anode catalysts in direct methanol fuel cells. Furthermore, it is also demonstrated that the nanoporous $Pt_{46}Ni_{54}$ nanowires could be promising materials for electrochemical detection of hydrogen peroxide.

References

1 S. Koh and P. Strasser, *J. Am. Chem. Soc.*, 2007, **129**, 12624.
2 Z. C. Liu, S. Koh, C. F. Yu and P. Strasser, *J. Electrochem. Soc.*, 2007, **154**, B1192.
3 P. Strasser, S. Koha and J. Greeley, *Phys. Chem. Chem. Phys.*, 2008, **10**, 3670.
4 N. Tian, Z. Y. Zhou, S. G. Sun, Y. Ding and Z. L. Wang, *Science*, 2007, **316**, 732.
5 F. Liu, J. Y. Lee and W. J. Zhou, *Small*, 2006, **2**, 121.
6 Y. L. Hou, H. Kondoh, R. C. Che, M. Takeguchi and T. Ohta, *Small*, 2006, **2**, 235.
7 C. Wang, Y. L. Hou, J. M. Kim and S. H. Sun, *Angew. Chem., Int. Ed.*, 2007, **46**, 6333.
8 G. Chen, D. G. Xia, Z. R. Nie, Z. Y. Wang, L. Wang, L. Zhang and J. J. Zhang, *Chem. Mater.*, 2007, **19**, 1840.
9 X. L. Tong, G. H. Zhao, M. C. Liu, T. C. Cao, L. Liu and P. Q. Li, *J. Phys. Chem. C*, 2009, **113**, 13787.
10 A. M. Yu, Z. J. Liang, J. H. Cho and F. Caruso, *Nano Lett.*, 2003, **3**, 1203.
11 B. S. Sherigara, W. Kutner and F. D'Souza, *Electroanalysis*, 2003, **15**, 753.
12 J. S. Huang, D. W. Wang, H. Q. Hou and T. Y. You, *Adv. Funct. Mater.*, 2008, **18**, 441.
13 S. J. Guo, S. J. Dong and E. K. Wang, *Small*, 2009, **5**, 1869.
14 J. Snyder, P. Asanithi, A. B. Dalton and J. Erlebacher, *Adv. Mater.*, 2008, **20**, 4883.
15 J. Erlebacher, M. J. Aziz, A. Karma, N. Dimitrov and K. Sieradzki, *Nature*, 2001, **410**, 450.
16 J. Erlebacher and K. Sieradzki, *Scr. Mater.*, 2003, **49**, 991.
17 Y. Ding, M. W. Chen and J. Erlebacher, *J. Am. Chem. Soc.*, 2004, **126**, 6876.
18 J. Weissmuller, R. C. Newman, H. J. Jin, A. M. Hodge and J. W. Kysar, *MRS Bull.*, 2009, **34**, 577.
19 S. H. Yoo and S. Park, *Adv. Mater.*, 2007, **19**, 1612.
20 T. Y. Shin, S. H. Yoo and S. Park, *Chem. Mater.*, 2008, **20**, 5682.
21 H. T. Liu, P. He, Z. Y. Li and J. H. Li, *Nanotechnology*, 2006, **17**, 2167.
22 D. V. Pugh, A. Dursun and S. G. Corcoran, *J. Mater. Res.*, 2003, **18**, 216.
23 H. J. Jin, D. Kramer, Y. Ivanisenko and J. Weissmuller, *Adv. Eng. Mater.*, 2007, **9**, 849.
24 J. S. Yu, Y. Ding, C. X. Xu, A. Inoue, T. Sakurai and M. W. Chen, *Chem. Mater.*, 2008, **20**, 4548.
25 L. Y. Chen, L. Zhang, T. Fujita and M. W. Chen, *J. Phys. Chem. C*, 2009, **113**, 14195.
26 Z. H. Zhang, Y. Wang, Z. Qi, W. H. Zhang, J. Y. Qin and J. Frenzel, *J. Phys. Chem. C*, 2009, **113**, 12629.
27 X. B. Ge, R. Y. Wang, P. P. Liu and Y. Ding, *Chem. Mater.*, 2007, **19**, 5827.

28 J. T. Zhang, H. Y. Ma, D. J. Zhang, P. P. Liu, F. Tian and Y. Ding, *Phys. Chem. Chem. Phys.*, 2008, **10**, 3250.
29 Z. Liu and P. C. Searson, *J. Phys. Chem. B*, 2006, **110**, 4318.
30 Q. F. Yi, A. C. Chen, W. Huang, J. J. Zhang, X. P. Liu, G. R. Xu and Z. H. Zhou, *Electrochem. Commun.*, 2007, **9**, 1513.
31 K. Koczkur, Q. F. Yi and A. C. Chen, *Adv. Mater.*, 2007, **19**, 2648.
32 P. Holt-Hindle, Q. F. Yi, G. S. Wu, K. Koczkur and A. C. Chen, *J. Electrochem. Soc.*, 2008, 155.
33 J. P. Wang, P. Holt-Hindle, D. MacDonald, D. F. Thomas and A. C. Chen, *Electrochim. Acta*, 2008, **53**, 6944.
34 C. X. Xu, L. Q. Wang, R. Y. Wang, K. Wang, Y. Zhang, F. Tian and Y. Ding, *Adv. Mater.*, 2009, **21**, 2165.
35 L. F. Liu, E. Pippel, R. Scholz and U. Gosele, *Nano Lett.*, 2009, **9**, 4352.
36 L. Liu, W. Lee, Z. Huang, R. Scholz and U. Gosele, *Nanotechnology*, 2008, **19**, 335604.
37 S. Parida, D. Kramer, C. A. Volkert, H. Rosner, J. Erlebacher and J. Weissmuller, *Phys. Rev. Lett.*, 2006, **97**, 035504.
38 K. Sieradzki and R. C. Newman, *J. Phys. Chem. Solids*, 1987, **48**, 1101.
39 B. Merzougui and S. Swathirajan, *J. Electrochem. Soc.*, 2006, **153**, A2220.
40 Z. L. Liu, X. Y. Ling, X. D. Su and J. Y. Lee, *J. Phys. Chem. B*, 2004, **108**, 8234.
41 E. Antolini, J. R. C. Salgado and E. R. Gonzalez, *Appl. Catal., B*, 2006, **63**, 137.
42 P. Mani, R. Srivastava and P. Strasser, *J. Phys. Chem. C*, 2008, **112**, 2770.
43 O. S. Wolfbeis, A. Durkop, M. Wu and Z. H. Lin, *Angew. Chem., Int. Ed.*, 2002, **41**, 4495.
44 C. M. Welch, C. E. Banks, A. O. Simm and R. G. Compton, *Anal. Bioanal. Chem.*, 2005, **382**, 12.
45 Nd. Merkulov., G. V. Zhutaeva, Na. Shumilov. and V. S. Bagotzky, *Electrochim. Acta*, 1973, **18**, 169.
46 J. Wang, M. Musameh and Y. H. Lin, *J. Am. Chem. Soc.*, 2003, **125**, 2408.
47 J. Wang and M. Musameh, *Anal. Chem.*, 2003, **75**, 2075.